

A population framework for predicting the proportion of people infected by the far-field airborne transmission of SARS-CoV-2 indoors

Christopher Iddon^a, Benjamin Jones^{a,*}, Patrick Sharpe^a, Muge Cevik^b,
Shaun Fitzgerald^c

^a*Department of Architecture and Built Environment, University of Nottingham,
Nottingham, UK*

^b*Department of Infection and Global Health, School of Medicine, University of St
Andrews, St Andrews, UK*

^c*Department of Engineering, Cambridge University, Cambridge, UK*

Abstract

The number of occupants in a space influences the risk of far-field airborne transmission of SARS-CoV-2 because the likelihood of having infectious and susceptible people both correlate with the number of occupants. This paper explores the relationship between occupancy and the probability of infection, and how this affects an individual person and a population of people. Mass-balance and dose-response models determine far-field transmission risks for an individual person and a population of people after sub-dividing a large *reference* space into 10 identical *comparator* spaces.

For a single infected person when the *per capita* ventilation rate is preserved, the viral dose received by an individual person in the *comparator* space is 10-times higher because the equivalent ventilation rate per infected person is lower.

*Corresponding author

Email address: benjamin.jones@nottingham.ac.uk (Benjamin Jones)

Preprint submitted to Indoor Air

December 3, 2021

However, accounting for population dispersion, such as the community prevalence, the probability of an infected person being present and uncertainty in their viral load, shows the probability of transmission increases with occupancy level. Also, far-field transmission is likely to be a rare event that requires a set of Goldilocks conditions that are *just right*, when mitigation measures have limited effect.

Therefore, resilient buildings should deliver the equivalent ventilation rate required by standards and increase the space volume per person, but also require reductions in the viral loads and the infection rate of the wider population.

Keywords: relative exposure index, ventilation, aerosols, transmission risk, viral load, COVID-19

1 **Nomenclature**

2 \bar{I} mean number of infected people present

3 \bar{D} mean dose in a space where one infected person is present

4 \bar{I} mean number of infected people in a space that contains a potential
5 transmission event

6 $\overline{P(R)_I}$ mean individual probability of infection occurring in a scenario

7 $\overline{P(R)}$ mean individual infection risk that occurs in all potential transmission
8 scenarios

9 ϕ total removal rate (s^{-1})

10 C community infections rate (%)

11 D dose (viable virions)

12 G emission rate of RNA copies (RNA copies s^{-1})

13 I number of infected people

14 K fraction of aerosol particles absorbed by respiratory tract

15 k reciprocal of the probability that a single pathogen initiates an infec-
16 tion

17 L viral load (RNA copies per ml of respiratory fluid)

18 N number of occupants

19 N_s number of susceptible people exposed

20 $N_s(I)$ number of susceptible people exposed in spaces that contain I infected
21 people

22 N_t number of transmissions in the entire population

23 $N_t(I)$ number of transmissions that occur in spaces that contain I infected
24 people

25 N_{pop} population size

26 $P(0 < I < N)$ probability of a space containing a potential transmission

27 $P(I)$ probability of I infected people present

28 $P(L)$ probability of a viral load

29 $P(R)$ individual probability of infection

30 $P(S)$ probability of a person being both susceptible and exposed to the virus

31 q_{sus} susceptible person respiratory rate ($\text{m}^3 \text{s}^{-1}$)

32 T exposure period (s)

33 V space volume (m^3)

34 v viable fraction

35 **1. Introduction**

36 Severe Acute Respiratory Syndrome Coronavirus 2 (SARS-CoV-2) is a
37 novel virus that causes COVID-19. In 2020, it spread rapidly worldwide

38 causing a pandemic. The transmission of the virus occurs when it is encap-
39 sulated within respiratory droplets and aerosols and inhaled by a susceptible
40 person [1]. These are most concentrated in the exhaled puff of an infected
41 person, which includes a continuum of aerosols and droplets of all sizes as a
42 multiphase turbulent gas cloud [2, 3]. The subsequent transport of infectious
43 aerosols from the exhaled puff occurs differently in outdoor and indoor en-
44 vironments. Outside, air movement disrupts the exhaled puff, a prodigious
45 space volume rapidly dilutes it [4], and ultra-violet (UV) light renders the
46 virus biologically non-viable over a short period of time [5]. Inside, the mag-
47 nitude of air movement is usually insufficient to disrupt the exhaled puff, a
48 finite space volume and lower ventilation rates concentrate aerosols in the air,
49 and there is usually less UV light [6]. Accordingly, transmission of the virus
50 occurs indoors more frequently than outdoors [7, 8], and inhaling the exhaled
51 puff at close contact is more likely to lead to an infective dose than when
52 inhaling indoor air at a distance where the virion laden aerosols are diluted.
53 This is consistent with the epidemiological understanding that SARS-CoV-2
54 is spread primarily by close contact where it might be possible to smell a
55 person's *coffee breath* [2, 3, 9, 10, 11]. However, it is still possible for a sus-
56 ceptible person to inhale an infective dose of aerosol borne virus, from shared
57 indoor air, known as *far-field* airborne transmission, and occurs at distances
58 of > 2 m. Far-field transmission is linked to several super spreading events
59 and is often correlated with poor indoor ventilation, long exposure times,
60 and respiratory activities that increase aerosol and viral emission, such as
61 singing [12, 13, 14].

62 The number of occupants in a space can have an influence on the risk of

63 airborne transmission because the likelihood of having infectious and suscep-
64 tible people both scale with the number of occupants. Therefore, it may be
65 advantageous to sub-divide a large space into a number of identical smaller
66 spaces to reduce the transmission risk. Here, the space volume and ventila-
67 tion rate per person is kept constant, and occupants are divided into smaller
68 groups of people. The impact of this strategy on virus transmission is not
69 obvious. On one hand, the lower occupancy space reduces the probability of
70 an infected person being present, and also reduces the number of susceptible
71 people who are exposed to infected people. On the other hand, the ventilation
72 rate per infected person is likely to be smaller in the smaller space, increasing
73 the transmission risk for any susceptible people present. Accordingly, this
74 paper explores the relationship between occupancy and the probability of in-
75 fection, and how this affects an individual person and a population of people.
76 We take a theoretical approach to consider the infection risk for the popula-
77 tion of a large space and compare it to the same population distributed in a
78 number of smaller identical spaces.

79 We first consider the infection risk for a person using an existing analytical
80 model [15] to predict the dose and the probability that the dose leads to
81 infection. We then consider the infection risk for two equal populations
82 distributed evenly in either the big space or a number of smaller spaces,
83 by considering the community infection rate and the probability of infection
84 from a viral dose.

85 Section 2 outlines the modelling approach and the input data. Section 3
86 considers the personal risks from sub-division and Section 4 considers the
87 risks for a population. Section 5 discusses factors that affect infection risk

88 and limitation of the work.

89 **2. Theoretical approach**

90 An analytical model is used to predict the dose of viral genome copies of
91 an individual person and associated individual and population infection risks
92 of infection.

93 *2.1. Dose and infection risk*

94 The mass-balance model of Jones *et al.* [15] is used to predict the num-
95 ber of RNA copies absorbed by the respiratory tract of a person exposed to
96 aerosols in well mixed air over a significant period of time and combined with
97 the viable fraction, v , to give a dose, D .

$$D \simeq \frac{K q_{sus} G T v}{\phi V} \quad (1)$$

98 Here, K is the fraction of aerosol particles absorbed by respiratory tract,
99 q_{sus} is the respiratory rate ($\text{m}^3 \text{s}^{-1}$), G is the emission rate of RNA copies
100 (RNA copies s^{-1}) and is a function of the respiratory activity (see Jones *et*
101 *al.*), T is the exposure period (s), ϕ is the total removal rate (s^{-1}), which
102 represents the sum of all removal by ventilation, surface deposition, biological
103 decay, respiratory tract absorption, and filtration, and V is the space volume
104 (m^3). The product ϕV can be considered to be an *equivalent* ventilation
105 rate. The approach is common and has been used by others to investigate
106 exposure in well mixed air [16, 17].

107 For a full description of the model, a discussion of uncertainty in suitable
108 inputs, and a sensitivity analysis see Jones *et al.* [15]. The analysis shows that

109 the most sensitive parameter is G , the rate of emission of RNA copies. G is a
110 function of the *viral load* in the respiratory fluid, L (RNA copies per ml) and
111 the volume of aerosols emitted, which in turn is a function of exhaled breath
112 rate and respiratory activity; see Appendix Appendix A. The distribution
113 of the viral load within the infected population is reported to be log-normal
114 by Yang *et al.* [4], Weibull by Chen *et al.* [18], and Gamma by Ke *et al.* [19].
115 This suggests that the true distribution is unknown and so we assume that
116 it is log-normally distributed with a mode of 10^7 RNA copies per ml using the
117 data of Chen *et al.* [20]; see Table 2 and Figure 1. We explore variations in
118 these values in Section 2.3 and discuss their origin and uncertainty in them
119 in Section 5.5. The probability of a viral load, $P(L)$, can then be determined
120 using the standard equation for the log-normal probability distribution func-
121 tion.

122 The dose can be used to estimate a probability of infection using a dose-
123 response curve. However, there is no dose-response curve for SARS-CoV-2.
124 A number of studies [21, 16, 22] apply a dose curve for the SARS-CoV-1 virus,
125 which is a typical dose curve for corona viruses, and so it is applied here.
126 There are obvious problems with this extrapolation and they are discussed
127 in Section 5.5. The probability of infection of an individual person, $P(R)$, is
128 given by

$$P(R) = 1 - e^{-D/k} \quad (2)$$

129 where, k is the reciprocal of the probability that a single pathogen initiates
130 an infection. We use a value of $k = 410$ following DeDiego *et al.*[23].

131 *2.2. Individual risk*

132 A Relative Exposure Index (REI) is used to compare exposure risk for
133 an individual person between two spaces following Jones *et al.* [15]. This
134 approach has already been used to inform national policy on the role of
135 ventilation in controlling SARS-CoV-2 transmission and to identify the ap-
136 propriate application of air cleaning devices [24, 25].

137 The REI is the ratio of the dose, D , received by a susceptible occupant
138 in each of two spaces using Equation 1 where the *reference* space is the
139 denominator and the *comparator* space is the numerator. An advantage
140 of using an REI is that uncertainty in the viral load of respiratory fluid
141 (RNA copies per ml), which is used to determine the viral emission rate, G
142 (RNA copies m^{-3}), and the unknown dose response, cancel allowing scenarios
143 to be compared. When the REI is > 1 the comparator space is predicted to
144 pose a greater risk to an individual susceptible occupant because they inhale
145 a larger dose in the comparator scenario, although the absolute risk that this
146 dose will lead to a probability of infection is not considered. Any space that
147 wishes to have a REI of unity or less, must at least balance the parameters
148 in Equation 1.

149 *2.3. Population infection risk*

150 A limitation of the REI is that it does not consider the probability of
151 encountering an infected person with the same viral load in each scenario.
152 The probability that a number of infected people, I , is present in a space,
153 $P(I)$, with a number of people present, N , is determined by considering the

154 community infections rate, C , and standard number theory for combinations.

$$P(I) = \frac{C^I(1 - C)^{(N-I)}N!}{I!(N - I)!} \quad (3)$$

155 The total number of transmissions that occur in a population, N_t , of N_{pop}
156 people, is the sum of the number of transmissions that occur in each trans-
157 mission scenario.

$$N_t = \sum_{I=1}^{N-1} N_t(I) \quad (4)$$

158 For a large population, the number of people infected in each space can be
159 given by the product of the number of susceptible people exposed, N_s , and
160 the mean individual probability of infection for a scenario, $\overline{P(R)}_I$.

$$N_t = \sum_{I=1}^{N-1} N_s(I)\overline{P(R)}_I \quad (5)$$

$$N_s(I) = P(I)\frac{N_{pop}}{N}(N - I) \quad (6)$$

161 where $N_s(I)$ denotes the number of susceptible people exposed in spaces
162 that contain I infected people, $P(I)$ is the probability that a space contains
163 I infected people, and $N_{pop}N^{-1}$ denotes the total number of spaces that
164 occur when a population N_{pop} is divided into groups of N people. Here, the
165 proportion of the population who are infected can be given by

$$PPI = \frac{N_t}{N_{pop}} = \sum_{I=1}^{N-1} P(I)\frac{N - I}{N}\overline{P(R)}_I \quad (7)$$

166 The exact solution for Equation 7 becomes increasingly difficult to eval-
167 uate as the space size increases. The calculation complexity is unlikely to
168 be justified given the uncertainties in both the modelling assumptions and
169 the available data. Therefore, simple approximations to the equation are
170 desirable.

171 One approach is to express the number of transmission events using a
172 single mean individual risk for all possible transmission scenarios. Here, the
173 *PPI* can be expressed as

$$PPI = P(S)\overline{P(R)} \quad (8)$$

174 where $P(S)$ is the proportion of the population who are both exposed and
175 susceptible, and $\overline{P(R)}$ is the average individual infection risk that occurs in
176 all potential transmission scenarios.

177 Transmission events can only occur when there are both one or more
178 infected people present in a space ($I > 0$) and one or more susceptible people
179 are present ($I < N$). It follows that the probability of a space containing a
180 potential transmission event is given by

$$P(0 < I < N) = 1 - C^N - (1 - C)^N \quad (9)$$

181 As the number of occupants tends to infinity, the probability that the space
182 contains a potential transmission event approaches one, and is equal to zero
183 for single occupancy spaces. This suggests that it may be better to partition
184 a large space; see Section 1. Likewise, the probability that a space contains
185 susceptible people can be minimised by reducing the community infections

186 rate, as long as the community infections rate is less than half. Furthermore,
187 each space contains $(N - I)$ susceptible people in it. This allows the prob-
188 ability that a user of the space is both susceptible and exposed to be given
189 by

$$P(S) = (1 - C) - (1 - C)^N \quad (10)$$

190 where $P(S)$ approaches the proportion of susceptible people in the wider
191 community as $N \rightarrow \infty$.

192 Evaluating the mean individual risk is non-trivial. Here an approximation
193 is used, where

$$\overline{P(R)} = \int_1^\infty P(L) \left(1 - e^{-\frac{D}{k}\bar{I}}\right) dL \quad (11)$$

194 Here $P(L)$ is the probability of a person having a viral load L , and \bar{I} denotes
195 the mean number of infected people in a space that contains a potential
196 transmission event, and is given by

$$\bar{I} = \frac{N(C - C^N)}{P(0 < I < N)} \quad (12)$$

197 This allows the proportion of people infected in a scenario to be approximated
198 by

$$PPI \approx P(S) \int_1^\infty P(L) \left(1 - e^{-\frac{D}{k}\bar{I}}\right) dL \quad (13)$$

199 and is further simplified by assuming that mean infection probabilities are

200 adequately described using a mean viral load, which can often be found
201 directly from the literature. Here

$$PPI \approx P(S) \left(1 - e^{-\frac{\bar{D}}{k}I}\right) \quad (14)$$

202 where \bar{D} is the mean dose received in the space where one infected person is
203 present.

204 *2.4. Scenarios*

205 The probabilities given in Section 2.3 can be used to consider how the
206 number of occupants may affect the relative exposure risk at population scale.
207 First, we define a reference space against which others are compared. This
208 space is an office, which is chosen because it is a common space that is well
209 regulated in most countries and has consistent occupancy densities. It has
210 an occupancy density of 10 m^2 per person, a floor to ceiling height of 3 m,
211 and an outdoor airflow rate of 10 l s^{-1} per person. There are 50 occupants
212 who are assumed to be continuously present for 8 hours breathing for 75%
213 and talking for 25%. Hereon it is known as the Big Office.

214 Then, we define a comparator space by subdividing the 50 person office
215 into 10 identical spaces. Each space preserves the occupancy density, the *per*
216 *capita* space volume, the outdoor airflow rate per person, and the air change
217 rate. Hereon each comparator space is known as the Small Office.

218 All scenario inputs are given in Table 1.

219 *2.5. Probabilistic estimates*

220 To investigate overdispersion in the model we use a Monte Carlo approach
221 that selects ten populations of 0.5×10^6 people and divides them into an equal

Table 1: Scenario inputs and calculations of individual risk.

	Big Office Reference	Small Office Comparator
Number of occupants, N	50	5
Space Volume, V (m ³)	1500	150
<i>Per capita</i> volume, $V N^{-1}$ (m ³ per person)		30
Air flow rate, ψV (l s ⁻¹)	500	50
Air change rate, ψ (h ⁻¹)		1.2
Removal rate, ϕ (h ⁻¹)		2.26
Equivalent ventilation rate, ϕV (l s ⁻¹)	942	94.2
Exposure time, T (h)		8
Dose constant, k [23]		410
Viable fraction, v (%)		100
Viral load (RNA copies per ml) [20]		10 ⁷
Respiratory activity, <i>breathing: talking</i> (%)		72:25
Viral emission rate, G (RNA copies per hour)		394
Respiratory rate, q_{sus} (m ³ h ⁻¹)		0.56
Community infection rate, C		1:100
Dose, D (viable virions inhaled)	0.245	2.450
REI	1	10

All values converted to SI units before application.

222 number of spaces, depending on the scenario; see Section 2.4. The predictions
 223 confirm the mathematics described herein, and identify the uncertainty in the
 224 number of transmissions that occur for each scenario; see Section 5.4. All
 225 inputs are given in Tables 1 and 2.

226 We do not explore uncertainty in other inputs because this has been done
 227 before [15] and to limit the exploration of uncertainty in the viral load and
 228 the community infection rate.

Table 2: Scenario inputs and calculations of population risk.

	Big Office Reference	Small Office Comparator
Viral load [20] (RNA copies per ml)	LN($2.1 \times 10^9, 2.0 \times 10^{10}$)	
$P(R)$ (%)	0.062	0.620
$P(I = 0)$ (%)	61	95
$P(0 < I < N)$ (%)	39	5
\bar{I}	1.27	1.02
$P(S)$ (%)	39	5
PPI (%)	1.59	0.43
TR		0.27

LN, log-normal(μ, σ)
All values converted to SI units before application.

229 3. Individual risk

230 The REI is the ratio of the dose predicted using Equation 1 for Big Office
 231 and Small Office; see Section 2.2. When the number of infected people and
 232 their respiratory activities, and the breathing rates of susceptible occupants,
 233 are identical in each space, the REI simplifies to a ratio of equivalent ven-
 234 tilation rates, ϕV . The equivalent ventilation rate is used to determine the
 235 steady state concentration of viable virions. Table 1 shows that the removal
 236 rate ϕ is identical in both spaces and so the REI becomes a simple ratio
 237 of the number of occupants. This suggests that, in the presence of a single
 238 infected person, the relative risk is 10 times higher in the Small Office. This
 239 occurs because the Small Office contains ten times fewer people than the Big
 240 Office, and therefore the ventilation rate *per infector* is ten times smaller.

241 The equivalent ventilation rate per person, $\phi V N^{-1}$, is identical in both
 242 spaces and, if it is desirable to preserve the equivalent ventilation per person

243 in two different spaces, the space volume per person must be preserved.

244 The removal rate, ϕ , includes the biological decay of the virus and the
245 deposition of aerosols onto surfaces. Both of these removal mechanisms are
246 space-volume dependent, and so their contribution to the removal of the
247 virus is greater in spaces with a larger volume. Therefore, increasing the
248 space volume per person also has the effect of reducing the REI. This has
249 obvious physical limitations and a simpler approach is to reduce the number
250 of people per unit of volume.

251 Equation 1 is used to calculate the dose of viable virions in each space
252 and Table 1 shows that the magnitudes of the doses are small. There is great
253 uncertainty in these values, attributable to modelling assumptions and in the
254 inputs given in Table 1, but an increase of an order of magnitude still leads
255 to a small dose. This fact is compounded by the value of unity for the viable
256 fraction, which has the effect that all RNA copies inhaled are viable, which
257 is unlikely. A viable fraction of unity was chosen because its true value is
258 currently unknown, and this assumption simplifies the analysis. The value
259 is clearly likely to be $\ll 100\%$ in reality, and so the actual doses would be
260 substantially lower than those estimated here. This suggests that far-field
261 transmission in buildings requires high viral emission rates, G , which are
262 likely to be a rare event.

263 The probability of an infection occurring when a susceptible occupant is
264 exposed to the dose reported in Table 1 is estimated using Equation 2 to
265 be $P(R) < 1\%$ for both spaces and is approximately 10 times greater in the
266 Small Office; see Table 2. Generally, this shows that the viral load has to
267 be greater in the Big Office than in the Small Office to achieve the same

268 $P(R)$ when $C < 1\%$. This is demonstrated by Figure 1, which describes the
269 relationship between the viral load in respiratory fluid (RNA copies per ml) in
270 each space attributable to any number of infected people and the consequent
271 $P(R)$ for a susceptible occupant, if the virus emission rate is assumed to be
272 linearly related to the viral load of the infected person.

273 For any viral load, L , the dose is calculated using Equation 1, and the
274 probability that it leads to an infection is calculated using Equation 2. This
275 creates a dose-response curve for both scenarios where factors that influence
276 the REI and, therefore, the dose, determine the viral loads necessary to lead
277 to a specific probability of infection. It also shows the relationship between
278 the viral load and the probability that a single infected person has that viral
279 load, $P(L)$. The dashed vertical lines show the viral load required to give
280 a 50% probability that the dose will lead to an infection for each scenario,
281 $P(R) = 50\%$. The area under the blue curve to the right of each vertical
282 line is the probability that the viral load of the infected person leads to
283 $P(R) \geq 50\%$. The probability is much smaller for the Big Office, which has
284 the lower REI. This probability that an infected person has a viral load that
285 leads to $P(R) \geq 50\%$ is small, suggesting that the most likely outcome is
286 $P(R) \leq 50\%$. There is great uncertainty in the magnitude of these values,
287 particularly in $P(R)$ and in the conversion of a viral load to a virus emission
288 rate (see Section 2), but significant increases in them do not change the
289 general outcomes of the analysis. More generally, increasing the number of
290 occupants in a space while preserving the *per capita* volume has the effect of
291 moving the $P(R)$ curve to the right in Figure 1 and towards the tail of the
292 $P(L)$ curve, which reduces the likelihood that infected people in the space

293 have a sufficient viral load.

294 The $P(L)$ distribution curve could be flattened and shifted to the left of
295 Figure 1 by reducing the viral load of the infected population; for example,
296 vaccination is shown to clear the virus from the body quicker in infected
297 vaccinated people, which at a population scale could flatten the distribution
298 of $P(L)$ [26]. However, different variants of the SARS-CoV-2 virus could
299 increase the viral load, or the proportion of viable virions, or the infectivity
300 of virions, and move the curve to the right of Figure 1 [27, 28]. Other
301 respiratory viruses will have different distributions of the viral load but the
302 principles described here can be applied to them too.

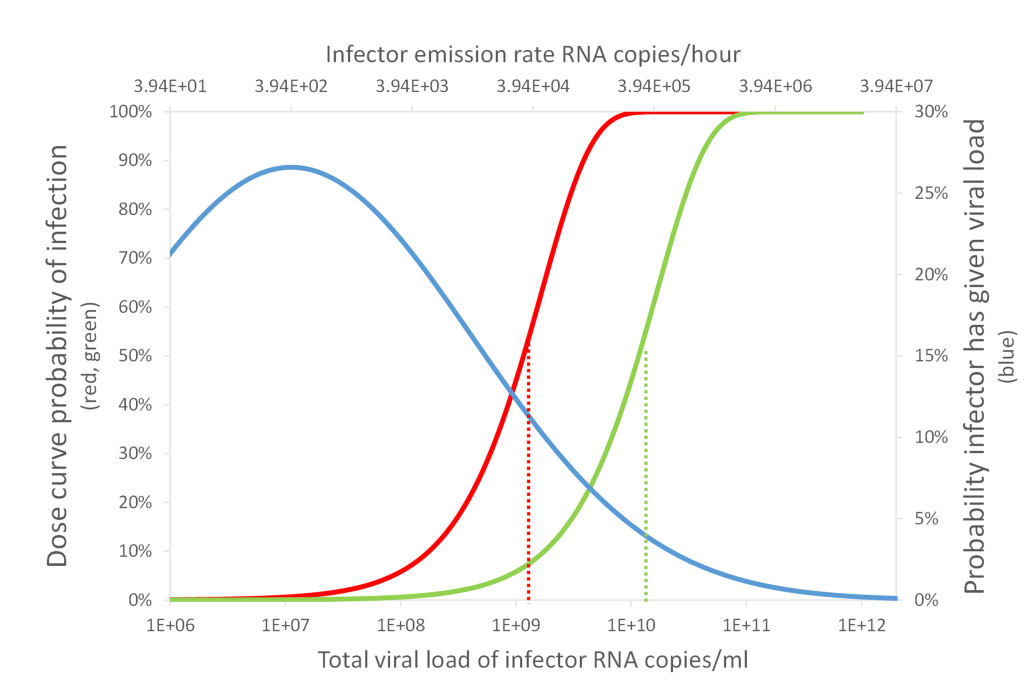


Figure 1: An indication of the relationship between the viral load, L , and the consequent probability of infection, $P(R)$, in the Big Office (green) and Small Office (red) for a susceptible occupant, and the probability of a single infected person having a viral load, $P(L)$, (blue). Dashed vertical lines indicate the viral load required for $P(R) = 50\%$.

303 4. Population risks

304 The analysis in Section 3 is underpinned by the assumption that there is
305 a single infected person in each space. When the community infection rate
306 (C) is known, Equation 3 can be used to estimate the probability that a
307 specific number of infected people are present. When $C = 1\%$, in the Big
308 Office $P(I = 0)$ is 61%, $P(I = 1)$ is 31%, and $P(I > 1)$ is 9%. For the Small
309 Office, $P(I = 0)$ is 95%, $P(I = 1)$ is 5%, and $P(I > 1)$ is negligible. This
310 shows that the Big Office is 8 times more likely to have an infected person
311 present than the Small Office, although Table 1 shows that the relative risk
312 is 10 times smaller in the Big Office than the Small Office when a single
313 infected person is present. However, it is much more likely that both spaces
314 do not have an infected person present, but when they are, the most likely
315 number of infected people is 1. The mean number of transmission scenarios
316 is just over 1 in both spaces when $C = 1\%$; see Equation 12.

317 Figure 1 shows the relationship between the probability of infection and
318 the probability of a person having a particular viral load. The viral load that
319 leads to an infection can be attributed to any number of infected people, but
320 the probability of having more than 1 infected person in a space is generally
321 small; see Equation 9. When only 1 infected person is assumed to be present,
322 Figure 1 also shows that the most probable viral loads are highly unlikely to
323 lead to an infection in either the Small Office or the Big Office. Therefore,
324 the infected person must have a significant viral load to infect susceptible
325 occupants, which is an improbable event. The infection risk for susceptible
326 occupants is lower in the Big Office than the Small Office when only 1 infected
327 person is assumed to be present.

328 Bigger spaces that preserve the *per capita* volume given in Table 1, and
329 where $N \gg 50$, have a higher probability of susceptible people, $P(S)$, and
330 infected people, $P(0 < I < N)$. The effect on the aerosol concentration and
331 the dose depends on the space volume per infected person, $V I^{-1}$, relative
332 to that of the Reference Space, the Big Office. If $V I^{-1}$ decreases, then the
333 aerosol concentration, the dose, and the probability of infection, $P(R)$, all
334 increase. Accordingly, spaces with a high volume per occupant have a lower
335 infection risk. Here, spaces with high ceilings or low occupancy densities are
336 advantageous.

337 An increase in C also increases the probabilities of the presence of infected
338 people, $P(0 < I < N)$, and susceptible people, $P(S)$, in any space. This
339 increases the total viral load, the dose, D , and the probability of infection,
340 $P(R)$. Accordingly, maintaining a low community infection rate is important.
341 It is worth noting that C may vary by region where the occupants are from,
342 or by a particular population demographic [29, 30]. Then, it is appropriate
343 to use C for that demographic, rather than using a national value. It is
344 possible to assess C by taking randomised samples from the population, such
345 as the UK Coronavirus (COVID-19) Infection Survey [31], which includes all
346 infected people at all stages of the disease. However, this survey includes
347 symptomatic people who are likely to be isolating and so the actual C is
348 likely to be lower.

349 The information in Figure 1 can be combined to determine the total
350 proportion of people infected, PPI , in a space for all viral loads as a function
351 of the probability that an individual person has a particular viral load, $P(L)$,
352 the probability of the risk of infection, $P(R)$, the probability of the presence

353 of susceptible people $P(S)$, and the average number of infected people, \bar{I} ; see
354 Equations 7 and 8.

355 Figure 2 shows the relationship between the proportion of people infected
356 and the viral load where the area under each curve is the proportion of the
357 entire population infected for a community infection rate of $C = 1\%$, and
358 assuming that two equal populations, one distributed evenly across a number
359 of Small Office scenarios and the other distributed evenly across a number
360 of Big Office scenarios. Figure 2 indicates that the probability of far-field
361 infection is $PPI = 0.43\%$ in the Small Office and $PPI = 1.59\%$ in the Big
362 Office, which shows that the risk is 3 to 4 times higher in the Big Office.
363 The absolute values are likely to be much smaller than those calculated here
364 because of the conservative assumptions used to estimate the viral emission
365 from viral load (see Section 2.1), so the PPI may well be $\ll 1\%$ in both spaces
366 using less conservative assumptions; see the Supplementary Materials¹. This
367 indicates that although there are benefits of subdividing for a population,
368 their magnitude needs to be considered against other factors, such as the
369 overall work environment, labour and material costs, and inadvertent changes
370 to the ventilation system and strategy.

371 A transmission ratio, TR , gives an indication of relative risk of infection
372 where

$$TR = PPI_{comparator} / PPI_{reference} \quad (15)$$

373 Here, the TR is 0.27.

¹[add SM link]

374 The uncertainties in all of the values given here are significant and so
375 it is not possible to be confident in the magnitude of the PPI or the TR ,
376 but testing the model with a range of assumptions enables an assessment of
377 general trends; for example, how increasing occupancy and preserving *per*
378 *capita* space volume and ventilation rates impact the risk of infection and
379 how different mitigation measures, such as increasing the ventilation rate,
380 affect the relative PPI . These are discussed in Section 5.

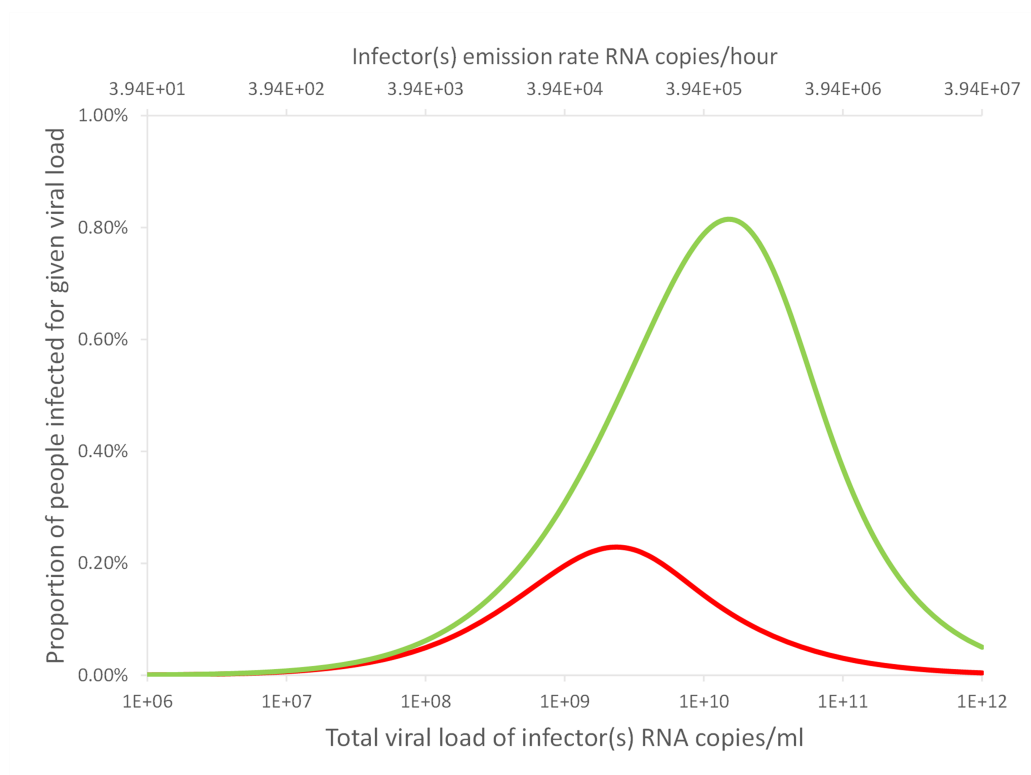


Figure 2: An indication of the relationship between the proportion of a population infected for a particular viral load when the community infection rate is $C = 1\%$. The area under the curve represents the total proportion of people infected for the Small Office (red) and the Big Office (green).

381 **5. Discussion**

382 *5.1. Ventilation and space volume*

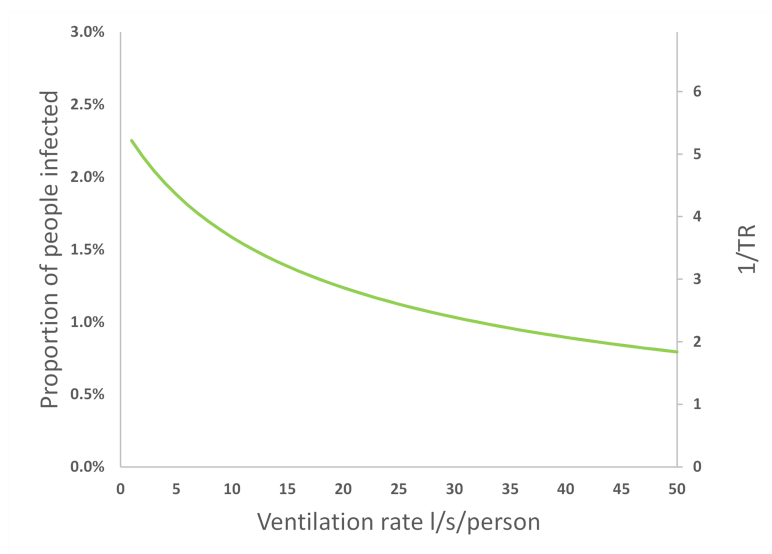


Figure 3: The effect of increasing the *per capita* ventilation rate, $\psi V N^{-1}$, in the Big Office on the *PPI* and the *TR* when the *per capita* ventilation rate in the Small Office is a constant 10l s^{-1} per person. All values are illustrative.

383 The quotient of the proportion of people infected in two scenarios gives
384 a Transmission Ratio, *TR*, see Equation 15. Increasing the *per capita* venti-
385 lation rate, $\psi V N^{-1}$, or space volume, $V N^{-1}$, in the Big Office reduces the
386 inverse of the *TR*. This has the effect of increasing the total removal rate, ϕ ,
387 and reducing the dose and the probability of infection; see Equation 1 and
388 Figure 3. However, there is a law of diminishing returns in reducing the *PPI*
389 by increasing the ventilation rate because the dose is inversely proportional
390 to ϕ . Therefore, it is more important to increase the ventilation rate in a
391 poorly ventilated space than in a well ventilated space because the change in
392 the *PPI* is greater.

393 A similar effect is seen when increasing the *per capita* space volume in the
394 Big Office while maintaining a constant *per capita* ventilation in both spaces.
395 This is because the dose is inversely proportional to volume. Furthermore,
396 the product of the space volume and the total removal rate, ϕV , is propor-
397 tional to the concentration of the virus in the air and, therefore, the infectious
398 dose. The *per capita* ventilation rate is constant in both spaces and so the
399 air change rate in the Big Office decreases as its volume increases. However,
400 this reduction is offset by the surface deposition and biological decay rates,
401 which remain constant and have a greater effect on the value of the equivalent
402 ventilation rate, ψV , as the space volume increases; see Section 2.1.

403 Equation 1 assumes a steady-state concentration of the virus has been
404 reached based on the assumption that the exposure time, T , is significant.
405 However, the time taken to reach the steady-state concentration in large
406 spaces may be significant and affects the dose over shorter exposure periods.
407 This is an example of the *reservoir effect*, the ability of indoor air to act as
408 a fresh-air reservoir and absorb the impact of contaminant emissions. The
409 greater the space volume, the greater the effect. These factors highlight the
410 benefits of increasing the *per capita* space volume.

411 5.2. Occupancy

412 Figure 4 shows the effect of increasing the number of occupants in the
413 Big Office while maintaining both the *per capita* space volume, $V N^{-1}$, and
414 ventilation rate, $\psi V N^{-1}$. As the number of occupants increases, the *PPI*
415 increases at an ever diminishing rate because the magnitude of the equivalent
416 ventilation rate, ϕV , increases at a greater rate than the probability of the
417 mean number of infected people, \bar{I} .

418 However, if the volume and ventilation rate remain constant as the oc-
419 cupancy increases, Figure 5 shows that the PPI and the inverse of the TR
420 increase linearly with occupancy. Here, the total removal rate, ϕ , remains
421 constant but the *per capita* space volume and ventilation rate reduce. There-
422 fore, the Big Office could have 14 occupants and have the same PPI as the
423 Small Office occupied by 5 people. Extrapolating to two identical popula-
424 tions of 140 people split into 28 Small Offices with 5 people in each, and 10
425 Big Offices with 14 people in each, the same PPI can be achieved.

426 This suggests that reducing the number of occupants in a space is the
427 most effective means of reducing the inverse of TR towards unity. To achieve
428 the same goal by increasing the ventilation rate or the *per capita* space volume
429 would require unfeasibly large increases in both.

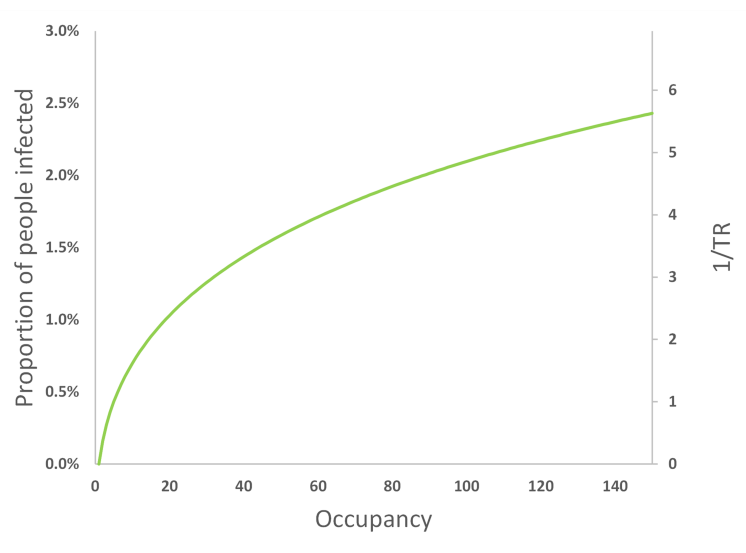


Figure 4: The effect of increasing the occupancy in the Big Office, where the space volume per person and ventilation rate per person is fixed at 30 m^3 and 10 l s^{-1} respectively, on the PPI (green) and TR (black). All values are illustrative.

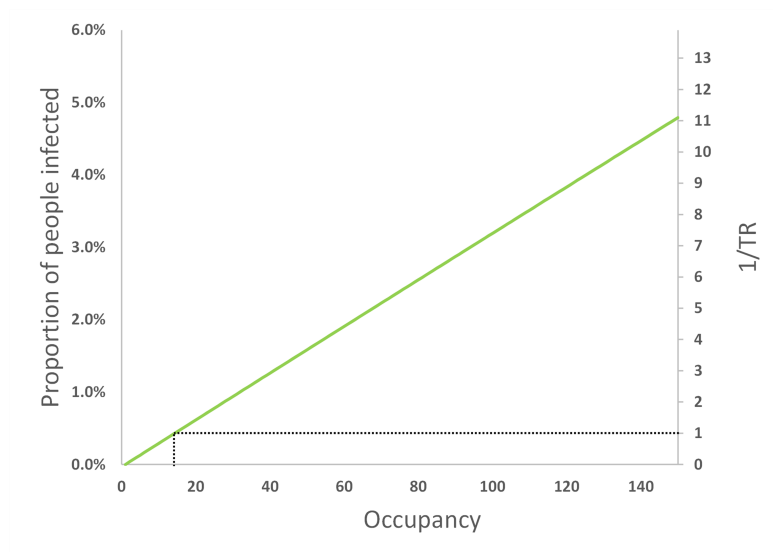


Figure 5: The effect of increasing the occupancy in the Big Office where the space volume and ventilation flow rate is fixed for a designed occupancy of 50 people (1500 m^3 and 500 l s^{-1} , respectively), on the PPI and TR . All values are illustrative.

430 5.3. Community infection rate

431 Figure 6 shows that the community infection rate, C , has a significant ef-
432 fect on the PPI and the TR . This is because it affects both the probability of
433 an infectious level of viral load, $P(L)$, and the probability of having suscepti-
434 ble people in a space, $P(S)$; see Equation 10. When $C > 1\%$, the probability
435 of transmission increases dramatically, suggesting that it strongly influences
436 the spread of the virus indoors. Figure 6 also shows that C only affects
437 the TR when the number of occupants, N , is less than the reciprocal of the
438 community infection rate in both spaces, $N < 1/C$. Thereafter, the TR is
439 constant irrespective of the community infection rate; see the Supplementary
440 Materials¹.

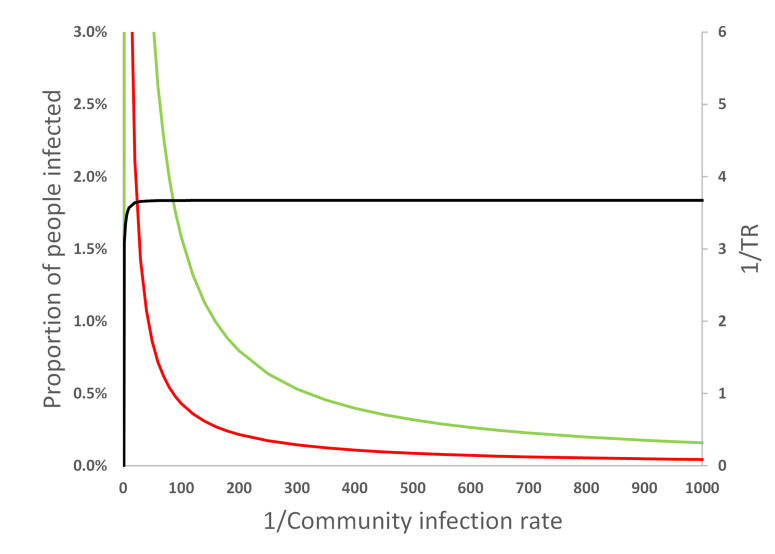


Figure 6: The effect of increasing the community infection rate , C , on the PPI in the Big Office (green) and the Small Office (red) and on the TR (black). All values are illustrative.

441 5.4. Overdispersion

442 The Monte Carlo approach described in Section 2.5 was used to interro-
443 gate every scenario and estimate the number of susceptible people infected
444 when an infected person is present in the Big Office. The Monte Carlo pre-
445 dictions indicate that at least one infected person was present 39% of the
446 time, confirming the value of $P(S)$ given in Table 2 determined using Equa-
447 tion 9. But, it also indicates that there was no transmission in 90% of the
448 scenarios. When a transmission does occur, the most common outcome is a
449 single transmission event; see Figure 7. This indicates that the dose inhaled
450 by all susceptible people is usually small enough not to lead to an infection.
451 At least 40 susceptible occupants are infected in the Big Office only 0.5%
452 of the cases where at least one infection occurs, given the assumptions in
453 Table 1. This suggests that so called *super-spreader* events, which occur by

454 far-field airborne transmission alone, are likely to be rare; see Figure 7. This
455 distribution reflects the overdispersion of transmission recorded for SARS-
456 CoV-2 and, although this work only considers one transmission route, similar
457 relationships between the viral load and the number of transmission events
458 may also be true for other transmission routes [11, 32, 33, 34, 35, 36, 37].

459 Applying the MC approach to the Small Office shows that the overdis-
460 persion is less pronounced because there are fewer susceptible people, which
461 limits the number of people who can be infected when an infected person has
462 a high viral load. Here, 0.2% of all scenarios, and 25% of scenarios with at
463 least one transmission, had 4 infections of susceptible people. In the Small
464 Office, all 4 susceptible occupants were infected in 46% of scenarios where at
465 least one person was infected.

466 There are very few epidemiological examples of high secondary COVID-
467 19 transmission events where $> 80\%$ of occupants in a scenario are infected
468 and this suggests that our assumptions over-estimate the viral emission rate.
469 One reason is the assumption that all genome copies are viable virions, which
470 is very unlikely.

471 Figure 7 shows that the frequency of the number of susceptible people
472 infected is highest at zero and decreases as the number of susceptible peo-
473 ple infected increases. However, the frequency later increases as the number
474 of susceptible people infected approaches the number of occupants. This
475 reflects the shape of the probability of infection curve in Figure 1 where a
476 point is reached when the viral load leads to the infection of all susceptible
477 people, and a higher viral load cannot infect more people. The phenomena
478 is a function of occupancy and is less likely to occur as the number of occu-

479 pants increases because the viral load required to infect all susceptible people
480 increases, assuming that the *per capita* space volume and ventilation rate are
481 constant.

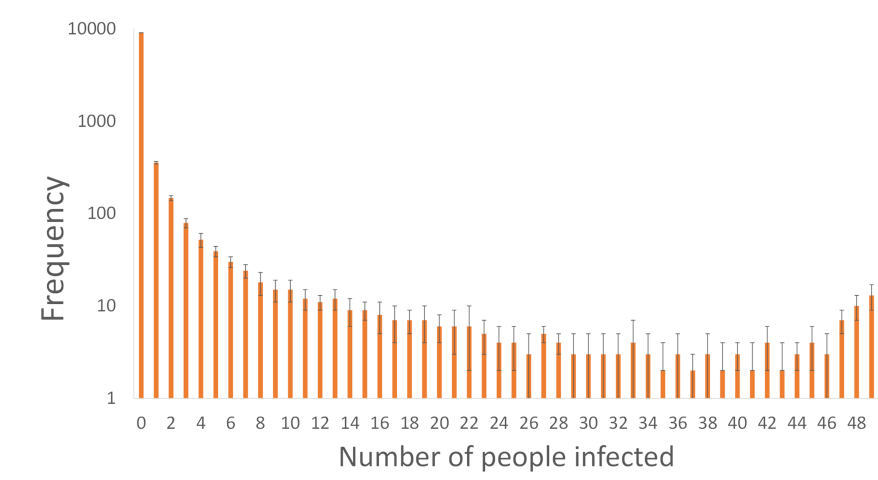


Figure 7: Uncertainty in the number of susceptible people infected in the Big Office Scenarios estimated using a Monte Carlo approach.

482 5.5. Limitations

483 Some limitations and uncertainties in this work have already been ad-
484 dressed, particularly those concerning the viral load and the dose-response
485 relationship. However, there are a number of other aspects that increase
486 uncertainty in it. Firstly, the models assume homogenous instantly mixed
487 indoor air to simplify the estimate of a dose. This assumption is unlikely to
488 be true in some spaces, especially in large spaces where the concentrations of
489 virions in the air is likely be a function of the distance from the infected per-
490 son, although it is unclear at which space volume this assumption becomes
491 less useful[38].

492 The approach described in Section 2 only considers the far-field trans-
493 mission of virus, and not near-field transmission, which is likely to be the
494 dominant route of transmission. The concentration of the virus in aerosols
495 and droplets per unit volume of air is several orders of magnitude greater
496 closer to the infected person at distances of < 2 m [3, 9]. However, it is likely
497 that the method of calculating the probability of viral load of infected people,
498 $P(L)$, is also important for the dose received by near-field transmission and
499 should be explored further in the future.

500 The distribution of viral load of an infected person around the median will
501 affect the probability of transmission. We apply a log-normal distribution,
502 see Section 2, but another, such as the Weibull distribution, will affect the
503 transmission probabilities differently.

504 The model also assumes a naïve population of susceptible people, and it
505 is unclear whether a higher infective dose is required for susceptible people
506 who have a greater immune response obtained from vaccination or a previous
507 infection. This paper does not consider the effect of the magnitude of the
508 dose on subsequent disease severity. However, a recent review suggests that
509 it is highly unlikely there is a link between dose and disease severity [39].

510 There is uncertainty in the dose-response relationship and the propor-
511 tion of people infected. In the absence of knowledge, we have assumed that
512 the dose-response curve for SARS-CoV-1 also applies to SARS-CoV-2; see
513 Section 2.1. The SARS-CoV-1 dose-response curve was generated from four
514 groups of inoculated transgenic mice [23] that were genetically modified to
515 express the human protein receptor of the SARS-CoV-1 virus. In three of the
516 groups all mice were infected and in the fourth one-third were infected. The

517 dose-response curve was fitted to data from these four groups and, although
518 it is limited, it is sufficient to assume that the curve follows the exponential
519 distribution rather than the Beta-Poisson distribution. A further limitation is
520 that the response of humans to a dose of SARS-CoV-1 may vary significantly
521 from that of transgenic mice. For a further discussion, see the Supplemental
522 Material¹. There is also uncertainty in the measurement of the viral load
523 used to challenge the study, and whether or not dose curves are valid for
524 predicting low probabilities of infection at very low virus titres. Other stud-
525 ies have used alternative dose-response curves for other coronaviruses, all of
526 which have similar uncertainties [21, 16].

527 The viral load of an infected person is the number of RNA copies per ml
528 of respiratory fluid, whereas the viral emission is the amount of RNA copies
529 per unit volume of exhaled breath; see Section 2.1. It has been established
530 that the viral load of an infected person increases in time from the moment of
531 infection and is highest just before, or at, the onset of COVID-19 symptoms.
532 As COVID-19 progresses the viral load reduces, normally within the first
533 week after the onset of symptoms [40, 41]. The viral load also varies between
534 people at any stage of the infection, which increases uncertainty in it [42, 43,
535 44, 19, 45, 18, 30, 37].

536 The viral load can be inferred from the *cycle threshold* values of real time
537 reverse transcription quantitative polymerase chain reaction (RT qPCR) na-
538 sopharyngeal (NP) swabs. This method assumes a direct correlation be-
539 tween the viral load of a swab and the viral load of respiratory fluid [46, 12].
540 RT qPCR is a semi-quantitative method because it requires a number of
541 amplification cycles to provide a positive signal of the SARS-CoV-2 genome,

542 which is proportional to the initial amount of viral genome in the original
543 sample. The cycle threshold is the number of polymerase chain reaction
544 cycles that are required before the chemical luminescence is read by the
545 equipment. The lower the starting amount of viral genome, the greater the
546 number of amplification cycles required. A calibrated standard curve is then
547 used to estimate the starting amount of viral genomic material. However,
548 the standard curve varies between test assays (investigative procedures) and
549 different RT qPCR thermal cyclers, the laboratory apparatus used to amplify
550 segments of RNA. This method also assumes a complete doubling of genetic
551 material after each cycle. The exponential relationship means that errors
552 in the calculation of the initial quantity of genomic material are orders of
553 magnitude higher for low cycle counts than for high cycle counts. Addition-
554 ally, if genomic data is taken from NP swabs, the estimated concentration of
555 genomic material per unit volume is often related to the amount of genomic
556 material in the buffer solution² in which NP swabs are eluted and used in
557 the assay, and not necessarily to the amount in a patient's respiratory fluid.
558 The amount of genomic material added to the buffer solution is dependent
559 on both a patient's viral load and the quality of the collection of the NP
560 sample, which is highly variable. Therefore, it is not possible to determine
561 absolute values of the viral load in a patient's respiratory fluid using this
562 method. However, data collected in this way is indicative of a range of vari-
563 ability, much of which is likely to be proportional to the viral load of the
564 person at the time the sample was collected. Some recent data suggests that

²a *buffer solution* resists a change in its pH when a small quantity of acid or alkali is added to it

565 the viral load of NP swabs may not reflect the amount of infectious material
566 present [19]. However, it is important to note that there are wide variations
567 in the measured genomic material in NP swabs and that the viral load in
568 respiratory fluid is likely to vary by several orders of magnitude.

569 There is clearly uncertainty in the viral load of respiratory fluid. There is
570 also uncertainty in the viral concentration in respiratory aerosols and droplets
571 and the distribution is currently unclear. Some studies suggest that the
572 number of virions in small aerosols with a diameter of $< 1 \mu\text{m}$ is higher
573 than would be expected given the viral concentration in the respiratory fluid
574 [47, 48] and that for SARS-CoV-2 there may be more genomic material in
575 the smallest aerosols [49].

576 There is high variability between people in the total volume of aerosols
577 generated per unit volume of exhaled breath, and it is dependent upon the
578 respiratory activity, such as talking and singing, and the respiratory capacity
579 [50, 51, 52, 53]. Coleman *et al.* [49] show that SARS-CoV-2 genomic material
580 is detectable in expired aerosols from *some* COVID-19 patients, but not all
581 of them because 41% exhaled no detectable genomic material. Singing and
582 talking generally produce more genomic material than breathing, but there
583 is large variability between patients. This suggests that respiratory activities
584 that have previously been shown to increase aerosol mass also increase the
585 amount of viral genomic material emitted. However, the viral concentration
586 in aerosols cannot be determined because the study did not measure the
587 mass of aerosols generated. Coleman *et al.* also show that the variability in
588 the amount of genomic material measured in expired aerosols is consistent
589 with the variability of viral loads determined using swabs and saliva [49].

590 Similarly, Adenaiye *et al.* [54] detected genomic material in aerosols from
591 patients infected with SARS-CoV-2 who provided a sample of exhaled air
592 when talking or singing. Genomic material was more frequently detected
593 in exhaled aerosols when the viral load of saliva or mid-turbinate swabs
594 was high; $> 10^8$ and $> 10^6$ RNA copies for mid-turbinate swabs and saliva
595 samples, respectively. Furthermore, they were able to culture viable virus
596 from $< 2\%$ of fine aerosol samples. It should be noted that one positive
597 sample was from a culture obtained from a fine aerosol sample that had an
598 amount of genomic material that was less than the detection limit of the
599 qRT PCR method that could be an artefact. Nevertheless, this provides
600 some evidence to support the epidemiological evidence that viable virus can
601 exist in exhaled aerosols.

602 Miller *et al.* suggests that around 1 : 1000 genome copies are likely to
603 be infectious virion [55, 12]. Adenaiye *et al.* use mid-turbinate swabs to
604 estimate that there are around 1 : 10^4 viable virus per measured genome
605 copies[54]. We make the assumption that all genome copies are viable virion,
606 which either over-estimates their infectiousness when using the Coleman *et*
607 *al.* data, or is similar to the assumption of Miller *et al.* if the viable virion
608 emission rate is in the order of 1000 virions per hour; see Appendix Appendix
609 A.

610 **6. Conclusions**

611 The number of occupants in a space can influence the risk of far-field air-
612 borne transmission that occurs at distances of > 2 m because the likelihood of
613 having infectious and susceptible people are both associated with the number

614 of occupants. Therefore, mass-balance and dose-response models are applied
615 to determine if it is advantageous to sub-divide a large reference space into
616 a number of identical smaller comparator spaces to reduce the transmission
617 risk for an individual person and for a population of people.

618 The reference space is an office with a volume of 1500 m^3 occupied by
619 50 people over an 8 hour period, and has a ventilation rate of 10 l s^{-1} per per-
620 son. The comparator space is occupied by 5 people and preserves the oc-
621 cupancy period and the *per capita* volume and ventilation rate. The dose
622 received by an individual susceptible person in the comparator Small Office,
623 when a single infected person is present, is compared to that in the reference
624 Big Office for the same circumstances to give a relative exposure index (REI)
625 with a value of 10 in the Small Office. This REI is a measure of the risk of
626 a space relative to the geometry, occupant activities, and exposure times of
627 the reference scenario and so it is not a measure of the probability of infec-
628 tion. Accordingly, when a single infected person is assumed to be present, a
629 space with more occupants is less of a risk for susceptible people because the
630 equivalent ventilation rate per infected person is higher.

631 The assumption that only one infected person is present is clearly prob-
632 lematic because, for a community infection rate of 1%, the most likely num-
633 ber of infected people in a 50 person space is zero. A transmission event
634 can only occur when there are both one or more infected people present in
635 a space and one or more susceptible people are present. The probability of
636 a transmission event occurring increases with the number of occupants and
637 the community infection rate; for example, the Big Office is over 12 times
638 more likely to have infected people present than the Small Office. However,

639 the geometry and ventilation rate in a larger space are non-linearly related to
640 the number of infected and susceptible people and so their relationship with
641 the probability of a transmission event occurring is also non-linear. These
642 effects are evaluated by considering a large population of people. But, this
643 introduces uncertainty in factors that vary across the population, such as the
644 viral load of an infected person, defined as the number of RNA copies per ml
645 of respiratory fluid. The viral load varies over time and between people at
646 any stage of the infection.

647 By applying a distribution of viral loads across a population of infected
648 people, secondary transmissions (new infections) are found to be likely to
649 occur only when the viral load is high, although the probabilities of this
650 occurring in the Big Office and the Small Office are low. This makes it
651 hard to distinguish the route of transmission epidemiologically. Generally,
652 the viral load must be greater in the Big Office than in the Small Office to
653 achieve the same proportion of the population infected when the community
654 infection rate is $\leq 1\%$. The viable fraction is unknown but a value of unity
655 was chosen for computational ease, yet the estimated doses and infection
656 probabilities are small. Therefore, it is likely that far-field transmission is a
657 rare event that requires a set of Goldilocks conditions that are *just right*.

658 There are circumstances where the magnitude of the total viral load of the
659 infected people is too high to affect the probability of secondary transmissions
660 by increasing ventilation and space volume. Conversely, when the total viral
661 load is very small, the dose so small that it is highly unlikely to lead to an
662 infection in any space irrespective of its geometry or the number of susceptible
663 people present. There is a law of depreciating returns for the dose and,

664 therefore, the probability of infection, and the ventilation rate because they
665 are inversely related. Accordingly, it is better to focus on increasing effective
666 ventilation rates in under-ventilated spaces rather than increasing ventilation
667 rates above those prescribed by standards, or increasing effective ventilation
668 rates using air cleaners, in already well-ventilated spaces.

669 There are significant uncertainties in the modelling assumptions and the
670 data used in the analysis and it is not possible to have confidence in the calcu-
671 lated magnitudes of doses or the proportions of people infected. However, the
672 general trends and relationships described herein are less uncertain and may
673 also apply to airborne pathogens other than SARS-CoV-2 at the population
674 scale. Accordingly, it is possible to say that there are benefits of subdividing
675 a population, but their magnitudes need to be considered against other fac-
676 tors, such as the overall working environment, labour and material costs, and
677 inadvertent changes to the ventilation system and strategy. However, it is
678 likely that the benefits do not outweigh the costs in existing buildings when
679 a less conservative viable fraction is used because it decreases the magnitude
680 of the benefits significantly. It is likely to be more cost-effective to consider
681 the advantages of partition when designing new resilient buildings because
682 the consequences can be considered from the beginning.

683 There are other factors that will reduce the risk of transmission in ex-
684 isting buildings. Local and national stakeholders can seek to maintain low
685 community infection rates, detect infected people with high viral loads using
686 rapid antigen tests and support to isolate them (see the Supplementary Ma-
687 terials³), reduce the variance and magnitude of the viral load in a population

³[[add SM link](#)]¹

688 by encouraging vaccination [30]. Changes can be made to the use of exist-
689 ing buildings and their services, such as reducing the occupancy density of a
690 space below the level it was designed for while preserving the magnitude of
691 the ventilation rate, reducing exposure times, and ensuring compliance with
692 ventilation standards.

693 **Acknowledgements**

694 The authors acknowledge the Engineering and Physical Sciences Research
695 Council (EP/W002779/1) who financially supported this work. They are also
696 grateful to Constanza Molina for her comments on this paper.

697 **Appendix A. Estimating viral emission from viral load**

698 We assume that the RNA copies per ml concentration is constant in aerosols
699 and in NP swabs and then we use the assumptions of Jones *et al.* [15] to con-
700 vert a NP viral load into a virus emission rate. This method follows Jones *et*
701 *al.* and is derived from the work of Morawska *et al.* who determine vol-
702 ume distribution aerosols for different respiratory activities, and is similar
703 to that used by Lelieveld *et al.* [15, 17, 53]. Table A.3 shows the estimated
704 virus emission rate for different respiratory activities when the viral load
705 is 10^7 RNA copies per ml. For comparison, median measured values of virus
706 emission in aerosols from Coleman *et al.* are given. These values were mea-
707 sured by collecting RNA copies from COVID-19 patients, where the median
708 cycle threshold, required to process diagnostic samples, was 16. [49].

709

Table A.3: Estimated emission rates from an infected person with a viral load of 10^7 RNA copies per ml compared to measured emission rates from patients with a median cycle threshold of 16 [49]

	Estimated RNA copies h^{-1}	Measured median RNA copies h^{-1}
Breathing	203	127
Voiced counting (talking)	967	1912
Vocalisation (singing)	6198	2856
Breathing:talking 25:75	394	573*

*calculated using measured values for breathing and talking.

710 Additionally, unpublished work by Adenaiye *et al.* measured viral genome
711 in patients infected by the SARS-CoV-2 alpha variant, who were breathing
712 and talking, in coarse ($> 5 \mu\text{m}$) and fine ($\leq 5 \mu\text{m}$) aerosols with a total geo-
713 metric mean of 1440 RNA copies h^{-1} and a maximum of 3×10^5 RNA copies h^{-1}
714 [54]. These are greater than the estimated values given in Table A.3, but the
715 viral load, measured by genome copies from mid-turbinate swabs, was gen-
716 erally orders of magnitude higher than 10^7 RNA copies per ml.

717 In Section 4, the inhaled dose is calculated for all possible viral loads.
718 Here, it should be noted that the calculated RNA copies emission rate is as-
719 sumed to be linearly related to the viral load of respiratory fluids, so that
720 a viral load of 10^8 RNA copies per ml has a ten-fold greater emission rate.
721 For comparison, a virus emission rate of 394 RNA copies h^{-1} (assumed for a
722 viral load of 10^7 RNA copies per ml) leads to an individual doses of around
723 2.2 RNA copies and 0.2 RNA copies for the Small Office and Big Office sce-
724 narios, respectively.

725 The calculated emission rate of viral genome for a viral load of 10^7 RNA copies per ml
726 is a reasonable fit to the Coleman *et al.* and Adenaiye *et al.* data. For further
727 details see the Supplementary Materials⁴.

⁴[add SM link]1

728 **References**

- 729 [1] C. C. Wang, K. A. Prather, J. Sznitman, J. L. Jimenez, S. S. Lakdawala,
730 Z. Tufekci, L. C. Marr, Airborne transmission of respiratory viruses, *Sci-*
731 *ence* 373 (6558) (2021) eabd9149. doi:10.1126/science.abd9149.
732 URL [https://www.sciencemag.org/lookup/doi/10.1126/science.](https://www.sciencemag.org/lookup/doi/10.1126/science.abd9149)
733 [abd9149](https://www.sciencemag.org/lookup/doi/10.1126/science.abd9149)
- 734 [2] L. Bourouiba, Turbulent Gas Clouds and Respiratory Pathogen Emis-
735 sions: Potential Implications for Reducing Transmission of COVID-19,
736 *JAMA - Journal of the American Medical Association* 323 (18) (2020)
737 1837–1838. doi:10.1001/jama.2020.4756.
- 738 [3] G. Cortellessa, L. Stabile, F. Arpino, D. Faleiros, W. van den Bos,
739 L. Morawska, G. Buonanno, Close proximity risk assessment for SARS-
740 CoV-2 infection, *Science of The Total Environment* 794 (2021) 148749.
741 doi:10.1016/j.scitotenv.2021.148749.
742 URL <https://doi.org/10.1016/j.scitotenv.2021.148749>
- 743 [4] Q. Yang, T. K. Saldi, P. K. Gonzales, E. Lasda, C. J. Decker, K. L.
744 Tat, M. R. Fink, C. R. Hager, J. C. Davis, C. D. Ozeroff, D. Muhlrاد,
745 S. K. Clark, W. T. Fattor, N. R. Meyerson, C. L. Paige, A. R. Gilchrist,
746 A. Barbachano-Guerrero, E. R. Worden-Sapper, S. S. Wu, G. R. Bris-
747 son, M. B. McQueen, R. D. Dowell, L. Leinwand, R. Parker, S. L.
748 Sawyer, Just 2 percent of sars-cov-2 positive individuals carry 90 per-
749 cent of the virus circulating in communities, *Proceedings of the National*
750 *Academy of Sciences* 118 (21) (2021) e2104547118. doi:10.1073/pnas.

751 2104547118.

752 URL <http://www.pnas.org/lookup/doi/10.1073/pnas.2104547118>

753 [5] P. Dabisch, M. Schuit, A. Herzog, K. Beck, S. Wood, M. Krause,
754 D. Miller, W. Weaver, D. Freeburger, I. Hooper, B. Green, G. Williams,
755 B. Holland, J. Bohannon, V. Wahl, J. Yolitz, M. Hevey, S. Ratnesar-
756 Shumate, The influence of temperature, humidity, and simulated sun-
757 light on the infectivity of SARS-CoV-2 in aerosols, *Aerosol Science*
758 *and Technology* 55 (2) (2021) 142–153. doi:10.1080/02786826.2020.
759 1829536.

760 URL [https://www.tandfonline.com/doi/full/10.1080/02786826.](https://www.tandfonline.com/doi/full/10.1080/02786826.2020.1829536)
761 2020.1829536

762 [6] Z. Liu, Q. Guo, L. Zou, H. Zhang, M. Zhang, F. Ouyang, J. Su, W. Su,
763 J. Xu, H. Lin, J. Sun, J. Peng, H. Jiang, P. Zhou, H. Zhen, T. Liu,
764 R. Che, H. Zeng, Z. Zheng, J. Yu, L. Yi, J. Wu, J. Chen, H. Zhong,
765 X. Deng, M. Kang, O. G. Pybus, M. Hall, K. A. Lythgoe, Viral infection
766 and transmission in a large well- traced outbreak caused by the Delta
767 SARS-CoV-2 variant, *Virological.org* (2021).

768 URL <https://virological.org/t/viral-infection-and-transmission-in-a-large-wel>
769 724

770 [7] T. C. Bulfone, M. Malekinejad, G. W. Rutherford, N. Razani, Out-
771 door Transmission of SARS-CoV-2 and Other Respiratory Viruses: A
772 Systematic Review, *The Journal of infectious diseases* 223 (4) (2021)
773 550–561. doi:10.1093/infdis/jiaa742.

774 [8] M. Weed, A. Foad, Rapid scoping review of evidence of outdoor trans-

- 775 mission of COVID-19, (pre-print) (2020). doi:10.1101/2020.09.04.
776 20188417.
- 777 [9] N. Zhang, W. Chen, P. T. Chan, H. L. Yen, J. W. T. Tang, Y. Li, Close
778 contact behavior in indoor environment and transmission of respiratory
779 infection, *Indoor Air* 30 (4) (2020) 645–661. doi:10.1111/ina.12673.
- 780 [10] SAGE, SARS-COV-2 Transmission routes and environments, Tech.
781 Rep. October, SAGE, UK (2020).
782 URL [https://assets.publishing.service.gov.uk/government/
783 uploads/system/uploads/attachment_data/file/933225/S0824_
784 SARS-CoV-2_Transmission_routes_and_environments.pdf](https://assets.publishing.service.gov.uk/government/uploads/system/uploads/attachment_data/file/933225/S0824_SARS-CoV-2_Transmission_routes_and_environments.pdf)
- 785 [11] K. Escandón, A. L. Rasmussen, I. I. Bogoch, E. J. Murray, K. Es-
786 candón, S. V. Popescu, J. Kindrachuk, COVID-19 false dichotomies
787 and a comprehensive review of the evidence regarding public health,
788 COVID-19 symptomatology, SARS-CoV-2 transmission, mask wear-
789 ing, and reinfection, *BMC Infectious Diseases* 21 (1) (2021) 710.
790 arXiv:arXiv:1011.1669v3, doi:10.1186/s12879-021-06357-4.
791 URL [https://osf.io/k2d84/https://bmcinfectdis.
792 biomedcentral.com/articles/10.1186/s12879-021-06357-4](https://osf.io/k2d84/https://bmcinfectdis.biomedcentral.com/articles/10.1186/s12879-021-06357-4)
- 793 [12] S. L. Miller, W. W. Nazaroff, J. L. Jimenez, A. Boerstra, S. J. Dancer,
794 J. Kurnitski, L. C. Marr, L. Morawska, C. Noakes, Transmission of
795 SARS-CoV-2 by inhalation of respiratory aerosol in the Skagit Valley
796 Chorale superspreading event, *Indoor Air* in press (2020). doi:doi.
797 org/10.1111/ina.12751.

- 798 [13] D. Hijnen, A. Marzano, K. Eyerich, C. GeurtsvanKessel, A. Giménez-
799 Arnau, P. Joly, C. Vestergaard, M. Sticherling, E. Schmidt, Sars-cov-2
800 transmission from presymptomatic meeting attendee, germany., Emerg-
801 ing infectious diseases 26 (8) (2020). doi:10.3201/eid2608.201235.
- 802 [14] L. M. Groves, L. Usagawa, J. Elm, E. Low, A. Manuzak, J. Quint, K. E.
803 Center, A. M. Buff, S. K. Kemble, Community Transmission of SARS-
804 CoV-2 at Three Fitness Facilities — Hawaii, June–July 2020, MMWR
805 Surveillance Summaries 70 (9) (2021) 316–320. doi:10.15585/mmwr.
806 mm7009e1.
- 807 [15] B. Jones, P. Sharpe, C. Iddon, E. A. Hathway, C. J. Noakes, S. Fitzger-
808 ald, Modelling uncertainty in the relative risk of exposure to the SARS-
809 CoV-2 virus by airborne aerosol transmission in well mixed indoor air,
810 Building and Environment 191 (October 2020) (2021) 107617. doi:
811 10.1016/j.buildenv.2021.107617.
812 URL <https://doi.org/10.1016/j.buildenv.2021.107617>
- 813 [16] H. Parhizkar, K. G. Van Den Wymelenberg, C. N. Haas, R. L. Corsi, A
814 Quantitative Risk Estimation Platform for Indoor Aerosol Transmission
815 of COVID-19, Risk Analysis 0 (0) (2021). doi:10.1111/risa.13844.
- 816 [17] J. Lelieveld, F. Helleis, S. Borrmann, Y. Cheng, F. Drewnick, G. Haug,
817 T. Klimach, J. Sciare, H. Su, U. Pöschl, Model calculations of aerosol
818 transmission and infection risk of covid-19 in indoor environments, Inter-
819 national Journal of Environmental Research and Public Health 17 (21)
820 (2020) 1–18. doi:10.3390/ijerph17218114.

- 821 [18] P. Z. Chen, N. Bobrovitz, Z. Premji, M. Koopmans, D. N. Fisman, F. X.
822 Gu, Heterogeneity in transmissibility and shedding SARS-CoV-2 via
823 droplets and aerosols, *eLife* 10 (2021) 1–32. doi:10.7554/eLife.65774.
- 824 [19] R. Ke, P. P. Martinez, R. L. Smith, L. L. Gibson, A. Mirza, M. Conte,
825 N. Gallagher, C. H. Luo, J. Jarrett, A. Conte, M. Farjo, K. K. O.
826 Walden, G. Rendon, C. J. Fields, R. Fredrickson, D. C. Edmonson,
827 M. E. Baughman, K. K. Chiu, J. Yedetore, J. Quicksall, A. N.
828 Owens, J. Broach, Daily sampling of early SARS-CoV-2 infection
829 reveals substantial heterogeneity in infectiousness, (pre-print) (2021).
830 doi:<https://doi.org/10.1101/2021.07.12.21260208>.
831 URL [https://www.medrxiv.org/content/10.1101/2021.07.12.](https://www.medrxiv.org/content/10.1101/2021.07.12.21260208v1)
832 [21260208v1](https://www.medrxiv.org/content/10.1101/2021.07.12.21260208v1)
- 833 [20] P. Z. Chen, N. Bobrovitz, Z. Premji, M. Koopmans, D. N. Fisman, F. X.
834 Gu, Sars-cov-2 shedding dynamics across the respiratory tract, sex, and
835 disease severity for adult and pediatric covid-19, *eLife* 10 (2021) e70458.
836 doi:10.7554/eLife.70458.
837 URL <https://doi.org/10.7554/eLife.70458>
- 838 [21] T. Watanabe, T. A. Bartrand, M. H. Weir, T. Omura, C. N. Haas,
839 Development of a dose-response model for sars coronavirus. risk analysis:
840 an official publication of the society for risk analysis, *Risk Anal* 30 (7)
841 (2010) 1129–1138. doi:10.1111/j.1539-6924.2010.01427.x.
- 842 [22] X. Zhang, J. Wang, Dose-response Relation Deduced for Coronaviruses
843 From Coronavirus Disease 2019, Severe Acute Respiratory Syndrome,
844 and Middle East Respiratory Syndrome: Meta-analysis Results and its

845 Application for Infection Risk Assessment of Aerosol Transmission, Clin-
846 ical Infectious Diseases 73 (1) (2020) 1–5. doi:10.1093/cid/ciaa1675.

847 [23] M. L. DeDiego, L. Pewe, E. Alvarez, M. T. Rejas, S. Perlman, L. En-
848 juanes, Pathogenicity of severe acute respiratory coronavirus deletion
849 mutants in hACE2 transgenic mice, Virology 376 (2) (2008) 379–389.
850 doi:<https://doi.org/10.1016/j.virol.2008.03.005>.

851 URL [https://www.sciencedirect.com/science/article/pii/](https://www.sciencedirect.com/science/article/pii/S004268220800175X)
852 [S004268220800175X](https://www.sciencedirect.com/science/article/pii/S004268220800175X)

853 [24] SAGE, Emg: Role of ventilation in controlling sars-cov-2 transmission,
854 Tech. Rep. September, SAGE, UK (2020).

855 URL [https://www.gov.uk/government/publications/](https://www.gov.uk/government/publications/emg-role-of-ventilation-in-controlling-sars-cov-2-transmission-30-september-2020)
856 [emg-role-of-ventilation-in-controlling-sars-cov-2-transmission-30-september-2020](https://www.gov.uk/government/publications/emg-role-of-ventilation-in-controlling-sars-cov-2-transmission-30-september-2020)

857 [25] C. Molina, C. Iddon, P. Sharpe, B. Jones, CIBSE relative exposure
858 index calculator (2021).

859 URL [https://www.cibse.org/coronavirus-covid-19/](https://www.cibse.org/coronavirus-covid-19/emerging-from-lockdown#5)
860 [emerging-from-lockdown#5](https://www.cibse.org/coronavirus-covid-19/emerging-from-lockdown#5)

861 [26] P. Y. Chia, S. W. X. Ong, C. J. Chiew, L. W. Ang, J.-M. Chavatte,
862 T.-M. Mak, L. Cui, S. Kalimuddin, W. N. Chia, C. W. Tan, L. Y. A.
863 Chai, S. Y. Tan, S. Zheng, R. T. P. Lin, L. Wang, Y.-S. Leo, V. J. Lee,
864 D. C. Lye, B. E. Young, Virological and serological kinetics of sars-cov-
865 2 delta variant vaccine-breakthrough infections: a multi-center cohort
866 study, (pre-print) (2021).

867 [27] A. Singanayagam, S. Hakki, J. Dunning, K. J. Madon, M. A. Crone,

- 868 A. Koycheva, N. Derqui-Fernandez, J. L. Barnett, M. G. Whitfield,
869 R. Varro, A. Charlett, R. Kundu, J. Fenn, J. Cutajar, V. Quinn,
870 E. Conibear, W. Barclay, P. S. Freemont, G. P. Taylor, S. Ahmad,
871 M. Zambon, N. M. Ferguson, A. Lalvani, A. Badhan, S. Dustan,
872 C. Tejpal, A. V. Ketkar, J. S. Narean, S. Hammett, E. McDermott,
873 T. Pillay, H. Houston, C. Luca, J. Samuel, S. Bremang, S. Evetts,
874 J. Poh, C. Anderson, D. Jackson, S. Miah, J. Ellis, A. Lackenby,
875 Community transmission and viral load kinetics of the SARS-CoV-2
876 delta (B.1.617.2) variant in vaccinated and unvaccinated individuals in
877 the UK: a prospective, longitudinal, cohort study, *The Lancet Infectious*
878 *Diseases* 3099 (21) (oct 2021). doi:10.1016/S1473-3099(21)00648-4.
879 URL [https://linkinghub.elsevier.com/retrieve/pii/
880 S1473309921006484](https://linkinghub.elsevier.com/retrieve/pii/S1473309921006484)
- 881 [28] D. W. Eyre, D. Taylor, M. Purver, D. Chapman, T. Fowler, K. Pouwels,
882 A. S. Walker, T. E. A. Peto, The impact of SARS-CoV-2 vaccination
883 on Alpha and Delta variant transmission, (pre-print) (2021).
884 URL [http://medrxiv.org/content/early/2021/09/29/2021.09.
885 28.21264260.abstract](http://medrxiv.org/content/early/2021/09/29/2021.09.28.21264260.abstract)
- 886 [29] M. Cevik, S. D. Baral, Networks of SARS-CoV-2 transmission., *Science*
887 (New York, N.Y.) 373 (6551) (2021) 162–163. doi:10.1126/science.
888 abg0842.
889 URL <http://www.ncbi.nlm.nih.gov/pubmed/34244400>
- 890 [30] L. Y. W. Lee, S. Rozmanowski, M. Pang, A. Charlett, C. Anderson,
891 G. J. Hughes, M. Barnard, L. Peto, R. Vipond, A. Sienkiewicz,

892 S. Hopkins, J. Bell, D. W. Crook, N. Gent, A. S. Walker, T. E. A.
893 Peto, D. W. Eyre, Severe Acute Respiratory Syndrome Coronavirus
894 2 (SARS-CoV-2) Infectivity by Viral Load, S Gene Variants and
895 Demographic Factors, and the Utility of Lateral Flow Devices to
896 Prevent Transmission, *Clinical Infectious Diseases* 6 (2021) 1–32.
897 doi:10.1093/cid/ciab421.
898 URL [https://academic.oup.com/cid/advance-article/doi/10.](https://academic.oup.com/cid/advance-article/doi/10.1093/cid/ciab421/6273394)
899 [1093/cid/ciab421/6273394](https://academic.oup.com/cid/advance-article/doi/10.1093/cid/ciab421/6273394)

900 [31] ONS, ONS Coronavirus (COVID-19) Infection Survey,
901 [https://www.ons.gov.uk/peoplepopulationandcommunity/healthandsocialcare/conditionsand](https://www.ons.gov.uk/peoplepopulationandcommunity/healthandsocialcare/conditionsanddiseases/coronavirus/covid-19-infection-survey)
902 (2021).

903 [32] Q. Bi, Y. Wu, S. Mei, C. Ye, X. Zou, Z. Zhang, X. Liu, L. Wei,
904 S. A. Truelove, T. Zhang, W. Gao, C. Cheng, X. Tang, X. Wu,
905 Y. Wu, B. Sun, S. Huang, Y. Sun, J. Zhang, T. Ma, J. Lessler,
906 T. Feng, Epidemiology and transmission of COVID-19 in 391 cases
907 and 1286 of their close contacts in Shenzhen, China: a retrospective
908 cohort study, *The Lancet Infectious Diseases* 20 (8) (2020) 911–919.
909 doi:10.1016/S1473-3099(20)30287-5.

910 [33] J. E. Lemieux, K. J. Siddle, B. M. Shaw, C. Loreth, S. F. Schaffner,
911 A. Gladden-Young, G. Adams, T. Fink, C. H. Tomkins-Tinch, L. A.
912 Krasilnikova, K. C. DeRuff, M. Rudy, M. R. Bauer, K. A. Lagerborg,
913 E. Normandin, S. B. Chapman, S. K. Reilly, M. N. Anahtar, A. E.
914 Lin, A. Carter, C. Myhrvold, M. E. Kemball, S. Chaluvadi, C. Cusick,
915 K. Flowers, A. Neumann, F. Cerrato, M. Farhat, D. Slater, J. B. Harris,

916 J. A. Branda, D. Hooper, J. M. Gaeta, T. P. Baggett, J. O'Connell,
917 A. Gnirke, T. D. Lieberman, A. Philippakis, M. Burns, C. M. Brown,
918 J. Luban, E. T. Ryan, S. E. Turbett, R. C. LaRocque, W. P. Hanage,
919 G. R. Gallagher, L. C. Madoff, S. Smole, V. M. Pierce, E. Rosenberg,
920 P. C. Sabeti, D. J. Park, B. L. MacInnis, Phylogenetic analysis of SARS-
921 CoV-2 in Boston highlights the impact of superspreading events, *Science*
922 371 (6529) (2021). doi:10.1126/science.abe3261.

923 [34] D. Miller, M. A. Martin, N. Harel, O. Tirosh, T. Kustin, M. Meir,
924 N. Sorek, S. Gefen-Halevi, S. Amit, O. Vorontsov, A. Shaag, D. Wolf,
925 A. Peretz, Y. Shemer-Avni, D. Roif-Kaminsky, N. M. Kopelman,
926 A. Huppert, K. Koelle, A. Stern, Full genome viral sequences inform
927 patterns of SARS-CoV-2 spread into and within Israel, *Nature Commu-*
928 *nications* 11 (1) (2020). doi:10.1038/s41467-020-19248-0.
929 URL <http://dx.doi.org/10.1038/s41467-020-19248-0>

930 [35] J. Riou, C. L. Althaus, Pattern of early human-to-human trans-
931 mission of Wuhan 2019 novel coronavirus (2019-nCoV), Decem-
932 ber 2019 to January 2020, *Eurosurveillance* 25 (4) (2020) 1–5.
933 doi:10.2807/1560-7917.ES.2020.25.4.2000058.
934 URL [http://dx.doi.org/10.2807/1560-7917.ES.2020.25.4.](http://dx.doi.org/10.2807/1560-7917.ES.2020.25.4.2000058)
935 [2000058](http://dx.doi.org/10.2807/1560-7917.ES.2020.25.4.2000058)

936 [36] S. Chaudhuri, P. Kasibhatla, A. Mukherjee, W. Pan, G. Morrison,
937 S. Mishra, V. K. Murty, Analysis of overdispersion in airborne trans-
938 mission of Covid-19, (pre-print) (2021).
939 URL <https://doi.org/10.1101/2021.09.28.21263801>

- 940 [37] A. Goyal, D. B. Reeves, E. F. Cardozo-Ojeda, J. T. Schiffer, B. T.
941 Mayer, Viral load and contact heterogeneity predict sars-cov-2 transmis-
942 sion and super-spreading events, *eLife* 10 (2021) 1–63. doi:10.7554/
943 *eLife*.63537.
- 944 [38] G. N. Sze To, C. Y. H. Chao, Review and comparison between the
945 wells–riley and dose-response approaches to risk assessment of infectious
946 respiratory diseases, *Indoor air* 20 (1) (2010) 2–16. doi:10.1111/j.
947 1600-0668.2009.00621.x.
- 948 [39] L. M. Brosseau, K. Escandón, A. K. Ulrich, A. L. Rasmussen, C. J. Roy,
949 G. J. Bix, S. V. Popescu, K. Moore, M. T. Osterholm, SARS-CoV-2
950 Dose, Infection, and Disease Outcomes for COVID-19 – A Review, *Clinical Infectious Diseases* 54 (2021) 1–54. doi:10.1093/cid/ciab903.
951 URL [https://academic.oup.com/cid/advance-article/doi/10.](https://academic.oup.com/cid/advance-article/doi/10.1093/cid/ciab903/6397523)
952 [1093/cid/ciab903/6397523](https://academic.oup.com/cid/advance-article/doi/10.1093/cid/ciab903/6397523)
- 954 [40] M. Cevik, K. Kuppalli, J. Kindrachuk, M. Peiris, *Virology, transmission,*
955 *and pathogenesis of SARS-CoV-2*, *The BMJ* 371 (2020) 1–6. doi:10.
956 1136/bmj.m3862.
- 957 [41] M. Cevik, M. Tate, O. Lloyd, A. E. Maraolo, J. Schafers, A. Ho,
958 SARS-CoV-2, SARS-CoV, and MERS-CoV viral load dynamics, du-
959 ration of viral shedding, and infectiousness: a systematic review and
960 meta-analysis, *The Lancet Microbe* 2 (1) (2021) e13–e22. doi:10.1016/
961 S2666-5247(20)30172-5.
962 URL [http://dx.doi.org/10.1016/S2666-5247\(20\)30172-5](http://dx.doi.org/10.1016/S2666-5247(20)30172-5)

- 963 [42] Y. Pan, D. Zhang, P. Yang, L. L. Poon, Q. Wang, Viral load of SARS-
964 CoV-2 in clinical samples, *The Lancet Infectious Diseases* 20 (4) (2020)
965 411–412. doi:10.1016/S1473-3099(20)30113-4.
966 URL [http://dx.doi.org/10.1016/S1473-3099\(20\)30113-4](http://dx.doi.org/10.1016/S1473-3099(20)30113-4)
- 967 [43] S. Karimzadeh, R. Bhopal, H. Nguyen Tien, Review of infective
968 dose, routes of transmission and outcome of COVID-19 caused
969 by the SARS-COV-2: comparison with other respiratory viruses–
970 CORRIGENDUM, *Epidemiology and Infection* 149 (2021) e116.
971 doi:10.1017/S0950268821001084.
972 URL [https://www.cambridge.org/core/product/identifier/
973 S0950268821001084/type/journal_article](https://www.cambridge.org/core/product/identifier/S0950268821001084/type/journal_article)
- 974 [44] R. Challen, E. Brooks-Pollock, J. M. Read, L. Dyson, K. Tsaneva-
975 Atanasova, L. Danon, Risk of mortality in patients infected with SARS-
976 CoV-2 variant of concern 202012/1: Matched cohort study, *The BMJ*
977 372 (2021) 1–10. doi:10.1136/bmj.n579.
- 978 [45] A. S. Walker, E. Pritchard, T. House, J. V. Robotham, P. J. Birrell,
979 I. Bell, J. Bell, J. Newton, J. Farrar, I. Diamond, R. Studley, J. Hay,
980 K.-D. Vihta, T. E. Peto, N. Stoesser, P. C. Matthews, D. W. Eyre,
981 K. Pouwels, Ct threshold values, a proxy for viral load in community
982 SARS-CoV-2 cases, demonstrate wide variation across populations and
983 over time, *eLife* 10 (jul 2021). doi:10.7554/eLife.64683.
984 URL <https://elifesciences.org/articles/64683>
- 985 [46] G. Buonanno, L. Stabile, L. Morawska, Estimation of airborne viral
986 emission: Quanta emission rate of SARS-CoV-2 for infection risk as-

- 987 assessment, *Environment International* 141 (May) (2020) 105794. doi:
988 10.1016/j.envint.2020.105794.
- 989 [47] D. K. Milton, M. P. Fabian, B. J. Cowling, M. L. Grantham, J. J.
990 McDevitt, Influenza Virus Aerosols in Human Exhaled Breath: Particle
991 Size, Culturability, and Effect of Surgical Masks, *PLoS Pathogens* 9 (3)
992 (2013). doi:10.1371/journal.ppat.1003205.
- 993 [48] P. Fabian, J. J. McDevitt, W. H. DeHaan, R. O. Fung, B. J. Cowling,
994 K. H. Chan, G. M. Leung, D. K. Milton, Influenza virus in human
995 exhaled breath: An observational study, *PLoS ONE* 3 (7) (2008) 5–10.
996 doi:10.1371/journal.pone.0002691.
- 997 [49] K. K. Coleman, D. J. W. Tay, K. S. Tan, S. W. X. Ong, T. S. Than,
998 M. H. Koh, Y. Q. Chin, H. Nasir, T. M. Mak, J. J. H. Chu, D. K. Milton,
999 V. T. K. Chow, P. A. Tambyah, M. Chen, K. W. Tham, Viral Load of
1000 Severe Acute Respiratory Syndrome Coronavirus 2 (SARS-CoV-2) in
1001 Respiratory Aerosols Emitted by Patients With Coronavirus Disease
1002 2019 (COVID-19) While Breathing, Talking, and Singing, *Clinical*
1003 *Infectious Diseases* 2 (Xx) (2021) 1–7. doi:10.1093/cid/ciab691.
1004 URL [https://academic.oup.com/cid/advance-article/doi/10.](https://academic.oup.com/cid/advance-article/doi/10.1093/cid/ciab691/6343417)
1005 1093/cid/ciab691/6343417
- 1006 [50] F. K. Gregson, N. A. Watson, C. M. Orton, A. E. Haddrell, L. P. Mc-
1007 Carthy, T. J. Finnie, N. Gent, G. C. Donaldson, P. L. Shah, J. D.
1008 Calder, B. R. Bzdek, D. Costello, J. P. Reid, Comparing aerosol concen-
1009 trations and particle size distributions generated by singing, speaking
1010 and breathing, *Aerosol Science and Technology* 55 (6) (2021) 681–691.

1011 doi:10.1080/02786826.2021.1883544.

1012 URL <https://doi.org/10.1080/02786826.2021.1883544>

1013 [51] G. R. Johnson, L. Morawska, The mechanism of breath aerosol forma-
1014 tion, *Journal of Aerosol Medicine and Pulmonary Drug Delivery* 22 (3)
1015 (2009) 229–237. doi:10.1089/jamp.2008.0720.

1016 [52] G. R. Johnson, L. Morawska, Z. D. Ristovski, M. Hargreaves,
1017 K. Mengersen, C. Y. Chao, M. P. Wan, Y. Li, X. Xie, D. Kato-
1018 shevski, S. Corbett, Modality of human expired aerosol size distri-
1019 butions, *Journal of Aerosol Science* 42 (12) (2011) 839–851. doi:
1020 10.1016/j.jaerosci.2011.07.009.

1021 [53] L. Morawska, G. R. Johnson, Z. D. Ristovski, M. Hargreaves,
1022 K. Mengersen, S. Corbett, C. Y. Chao, Y. Li, D. Katoshevski, Size
1023 distribution and sites of origin of droplets expelled from the human res-
1024 piratory tract during expiratory activities, *Journal of Aerosol Science*
1025 40 (3) (2009) 256–269. doi:10.1016/j.jaerosci.2008.11.002.

1026 [54] O. O. Adenaiye, J. Lai, P. J. B. de Mesquita, F. Hong, S. Youssefi,
1027 J. German, S.-H. S. Tai, B. Albert, M. Schanz, S. Weston, J. Hang,
1028 C. Fung, H. K. Chung, K. K. Coleman, N. Sapoval, T. Treangen,
1029 I. M. Berry, K. Mullins, M. Frieman, T. Ma, D. K. Milton, Infec-
1030 tious SARS-CoV-2 in Exhaled Aerosols and Efficacy of Masks During
1031 Early Mild Infection, (pre-print) (2021). arXiv:2021.08.13.21261989,
1032 doi:<https://doi.org/10.1101/2021.08.13.21261989>.
1033 URL <https://doi.org/10.1101/2021.08.13.21261989>

1034 [55] V. M. Corman, I. Eckerle, T. Bleicker, A. Zaki, O. Landt, M. Eschbach-
1035 Bludau, S. van Boheemen, R. Gopal, M. Ballhause, T. M. Bestebroer,
1036 D. Muth, M. A. Müller, J. F. Drexler, M. Zambon, A. D. Osterhaus,
1037 R. M. Fouchier, C. Drosten, Detection of a novel human coronavirus by
1038 real-time reverse-transcription polymerase chain reaction, Eurosurveil-
1039 lance 17 (39) (2012) 1–6. doi:10.2807/ese.17.39.20285-en.
1040 URL <http://dx.doi.org/10.2807/ese.17.39.20285-en>